A Water-Miscible Quinone Flow Battery with High Volumetric Capacity and Energy Density

A Water-Miscible Quinone Flow Battery with High Volumetric Capacity and Energy Density

Shijian Jin,[▽,†] Yan Jing,[▽,‡] David G. Kwabi,[†,§] Yunlong Ji,[‡] Liuchuan Tong,[‡] Diana De Porcellinis,[†] Marc-Antoni Goulet,[†] Daniel A. Pollack,[#] Roy G. Gordon,[†,‡,] and Michael J. Aziz[†,*]*

[▽] Shijian Jin and Yan Jing contributed equally.

† John A. Paulson School of Engineering and Applied Sciences, Harvard University, Cambridge, MA 02138, USA

‡ Department of Chemistry and Chemical Biology, Harvard University, Cambridge, MA 02138, USA

§ Present Address: Department of Mechanical Engineering, University of Michigan, Ann Arbor, MI 48109

Department of Physics, Harvard University, Cambridge, MA 02138, USA

* To whom correspondence should be addressed: gordon@chemistry.harvard.edu (Roy G. Gordon); maziz@harvard.edu (Michael J. Aziz).

Abstract:

A water-miscible anthraquinone with polyethylene glycol (PEG)-based solubilizing groups is introduced as the redox-active molecule in a negative electrolyte (negolyte) for aqueous redox flow batteries, exhibiting the highest volumetric capacity among aqueous organic negolytes. We synthesized and screened a series of PEG-substituted anthraquinones (PEGAQs) and carefully studied one of its isomers, namely 1,8-bis(2-(2-(2-hydroxyethoxy)ethoxy)ethoxy)anthracene-9,10-dione (AQ-1,8-3E-OH), which has high electrochemical reversibility and is completely miscible in water of any pH. A negolyte containing 1.5 M AQ-1,8-3E-OH, when paired with a ferrocyanide-based positive electrolyte across an inexpensive, non-fluorinated permselective polymer membrane at pH 7, exhibits an open-circuit potential of 1.0 V, a volumetric capacity of 80.4 Ah/L, and an energy density of 25.2 Wh/L.

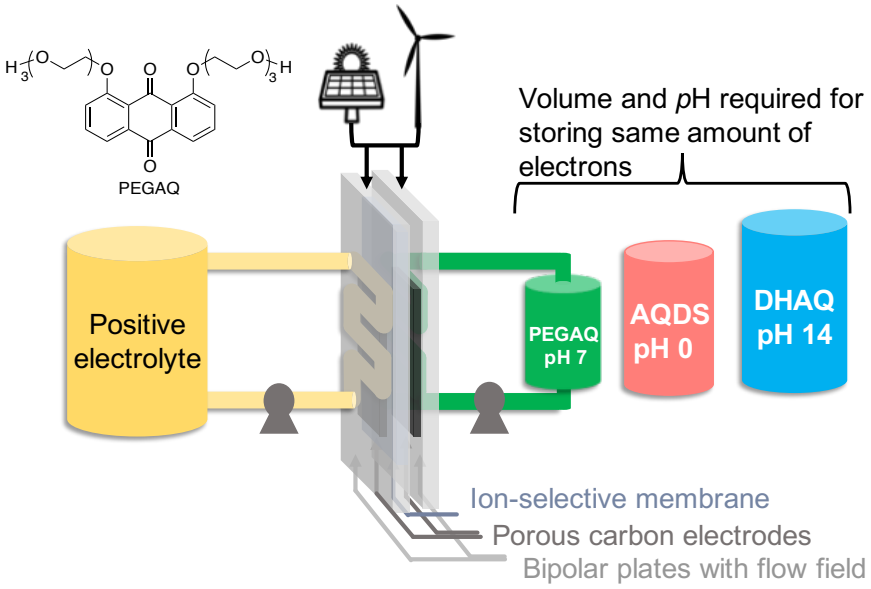

Renewable energy resources such as solar and wind energy are expected to replace fossil fuels for generating electricity[1]. However, the intermittent availability of renewable energy hampers its deep penetration into the electrical grid[2]. Safe, low-cost grid-scale energy storage could solve this problem[3]. Aqueous redox flow batteries (ARFBs) featuring low-cost and non-flammable electrolytes, as well as decoupled energy/power scaling, are particularly suitable for storing massive amounts of electricity generated from renewables[4, 5]. The vanadium redox flow battery has been the most developed ARFB, but the high price and low abundance of vanadium limits its widespread deployment[6, 7]. Redox-active organic molecules comprising earth abundant elements such as C, H, O, and N are potentially more cost-effective[8]and scalable. Moreover, the structural diversity and tunability of organics allows chemists to design molecules with important properties such as high solubility, fast kinetics, appropriate redox potentials, and high stability.

The potential cost of organic redox molecules has been projected to be extremely low[9, 10]. Recently, organic molecules with very long projected lifetimes have been developed as negative electrolyte (negolyte) molecules in ARFBs[11-14]. However, these organic molecules tend to have lower solubilities than vanadium species, resulting in considerably lower volumetric capacities for the resulting electrolytes[15]. Although the energy capacity can be scaled up by increasing the volume of electrolyte reservoirs, the size of electrolyte reservoirs may be constrained by available space and cost. Therefore, besides safety, low material cost, and long lifetime, storing as many electrons as possible per unit volume, *i.e.*, having a high volumetric capacity, is another valuable attribute for electrolytes, particularly where ARFBs are deployed in high population-density areas. In such cases, the physical space used for accommodating electrolyte tanks may contribute significantly to the total capital cost of ARFBs[16]. One strategy is to increase the aqueous solubility of redox active materials (RAMs). Ionic groups such as $-SO_3^-$ [13, 15, 17, 18], $-O^-$ [9, 19], $-COO^-$ [11, 15, 20, 21], $-PO_3^{2-}$ [14], and $-NR_3^+$ [12, 20] have been tethered to RAMs such as quinones, viologen, phenazine, ferrocene, and (2,2,6,6-Tetramethylpiperidin-1-yl)oxyl (TEMPO) to increase solubility; and molecules

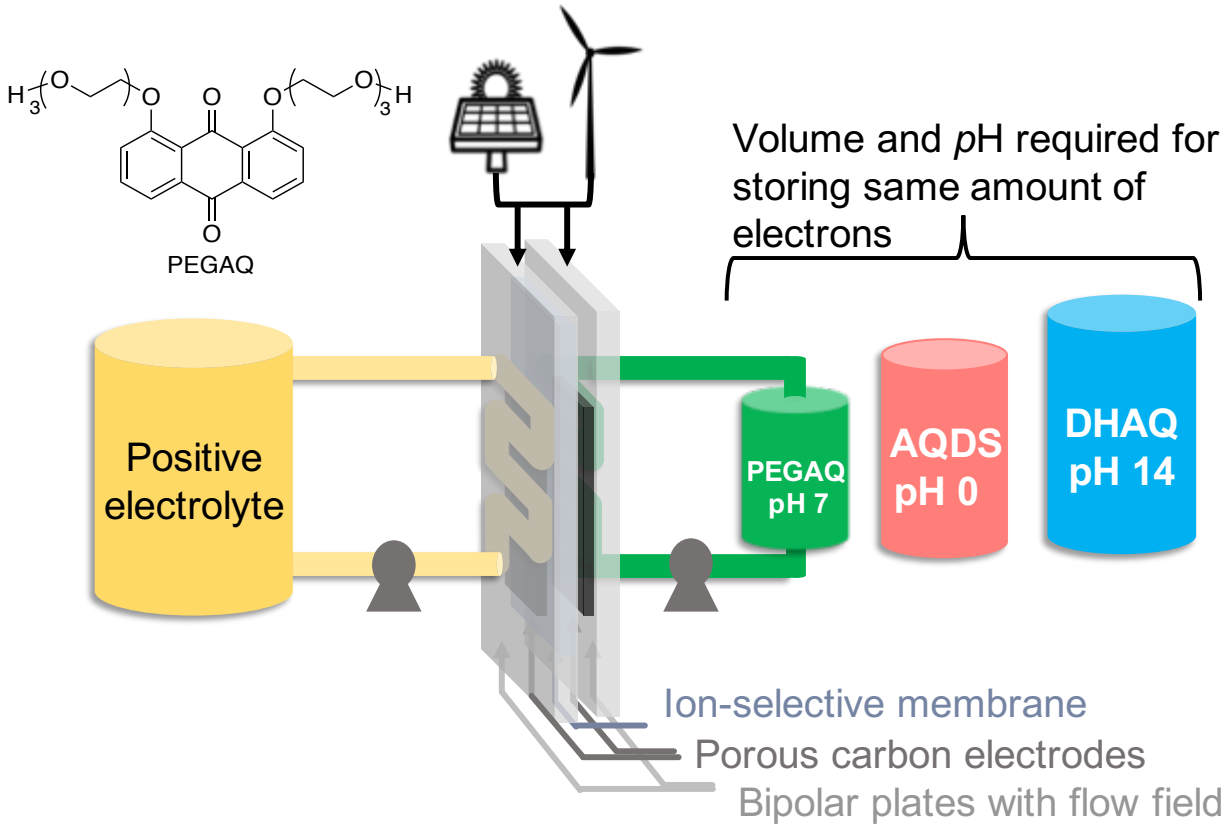

Figure 1 | A schematic flow battery with three different negative electrolytes (negolyte) PEGAQ, AQDS[18], and DHAQ[22]. The pH and volume required to store the same number of electrons are highlighted for each.

bearing these functional groups can demonstrate >1 M electron-storing capability. Frequently the solubility is heavily dependent on the electrolyte pH, and corresponding flow cells must be operated within certain pH ranges to achieve adequate capacity; otherwise RAMs precipitate due to changes in the protonation state or decomposition of ionic groups.

In this work, we incorporate a non-ionic but water-miscible motif, *i.e.*, tri-ethylene glycol, into an anthraquinone through the well-developed one-step Williamson ether synthesis, and report a water-miscible RAM, 1,8-bis(2-(2-(2-hydroxyethoxy)ethoxy)ethoxy)anthracene-9,10-dione (**AQ-1,8-3E-OH**) as a negolyte (Figure 1). Its pH-independent water miscibility enables us to prepare 1.5 M **AQ-1,8-3E-OH** at pH 7 and demonstrate a volumetric capacity of 80.4 Ah/L, which is the highest volumetric capacity reported to date among all aqueous organic negolytes (Figure 2). Pairing the negolyte with a 1.5 M ferrocyanide positive electrolyte (posolyte) at pH 7, our flow cell exhibits an open-circuit voltage of 1.0 V and an energy density of 25.2 Wh/L, which is one of the highest energy densities among all organic aqueous or non-aqueous flow batteries and is even comparable with most vanadium flow batteries.

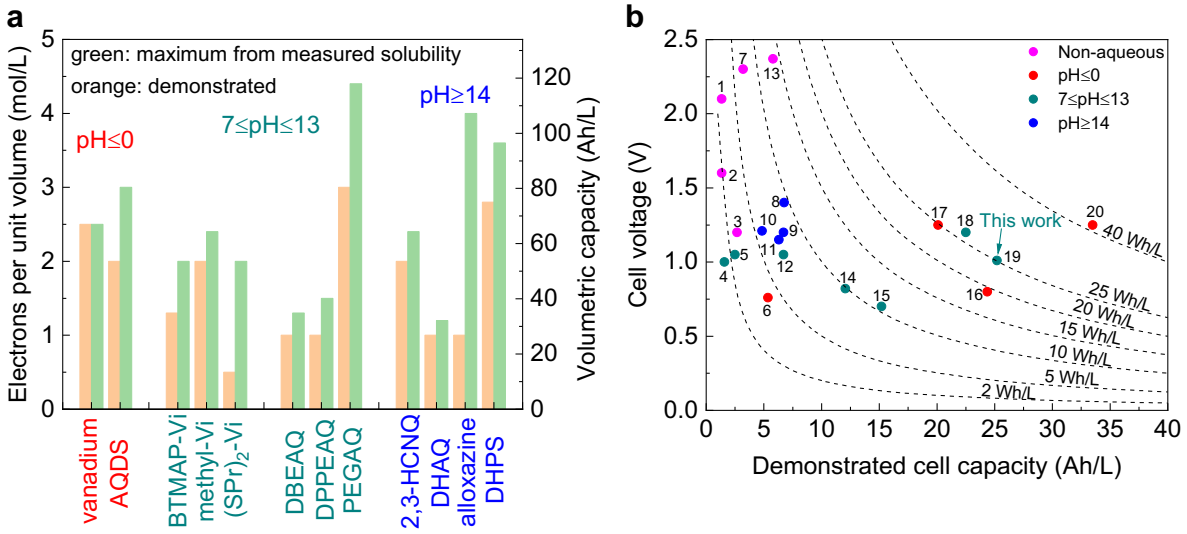

Figure 2 | The electrons stored per unit/volumetric capacity of negolytes and comparisons of demonstrated cell capacity/energy densities. (a) From left to right: in strong acid (pH<=0): vanadium[7], AQDS[18]; neutral (pH=~7): BTMAP-Vi[12], Methyl-Vi[20], (SPr)$_2$-Vi[17]; near neutral (7<=pH<=13): DBEAQ[11], DPPEAQ[14], PEGAQ (AQ-1,8-3E-OH); in strong base (pH>=14): 2,3-HCNQ[21], DHAQ[19], alloxazine[23], DHPS[15]. The orange bars represent demonstrated values in flow cells; the green bars represent maximum values calculated from measured solubilities. (b) The redox couples are listed as negolyte/posolyte. 1. V(acac)$_3$/V(acac)$_3$[24]; 2. FL/DMPZ[25]; 3. Methyl-ViTFSI/FcNTFSI[26]; 4. DPPEAQ/K$_4$Fe(CN)$_6$[14]; 5. DBEAQ/K$_4$Fe(CN)$_6$[11]; 6. AQS/BQDS[27]; 7. MePh/DBMMB[28]; 8. DHPS/K$_4$Fe(CN)$_6$[15]; 9. DHAQ/K$_4$Fe(CN)$_6$[22]; 10. DHBQ/K$_4$Fe(CN)$_6$[9]; 11. Alloxazine/K$_4$Fe(CN)$_6$[23]; 12. Methyl-Vi/FcNCl[29]; 13. FL/DBMMB[30]; 14. (SPr)$_2$-Vi/(NH$_4$)$_4$Fe(CN)$_6$[13]; 15. BTMAP-Vi/BTMAP-Fc[12]; 16. AQDS/HBr[31]; 17. Vanadium/vanadium (supporting electrolyte: H$_2$SO$_4$)[32]; 18. Methyl-Vi/TEMPTMA[20]; 19. PEGAQ/K$_4$Fe(CN)$_6$:Na$_4$Fe(CN)$_6$ (1:1); 20. vanadium/vanadium (supporting electrolyte: H$_2$SO$_4$/HCl mixture)[7].

[7]hydroxyethoxy)ethoxy)ethoxy)anthracene-9,10-dione (AQ-*n,m*-3E-OH) and 1,8-bis(2-(2-(2-methoxyethoxy)ethoxy)ethoxy)anthracene-9,10-dione (AQ-1,8-3E-OCH$_3$) through one-step Williamson etherification[33] (Scheme 1) (^{1}H and ^{13}C NMR spetra in Figure S1-S2). After measuring their solubilities (Figure S3) and evaluating reaction kinetics via cyclic voltammetry (CV) (See Supporting Information, Solubility Measurements, pp. 11-13, and Electochemical Characterization, pp. 12-14, for more details), we set out to further investigate the electrochemical properties of **AQ-1,8-3E-OH** for use as the RAM in a negolyte due to its high solubility and rapid kinetics (Figure S6-S8).

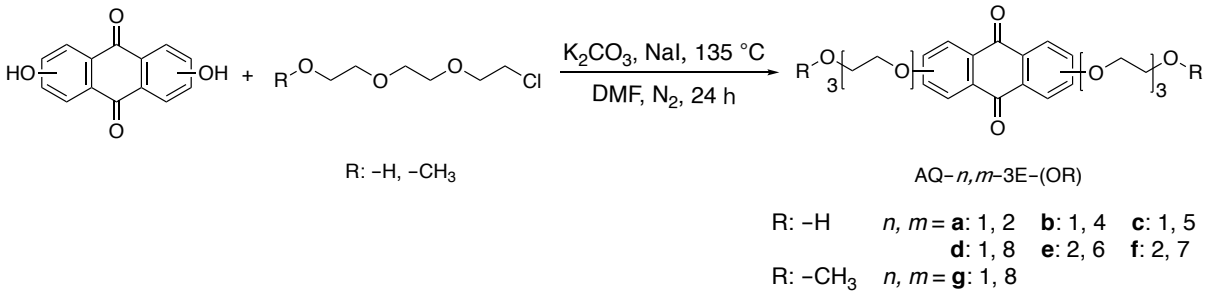

Scheme 1 | Synthetic conditions of PEGylated anthraquinone isomers through one-step Williamson etherification.

Based on the CV results, the reduction potential ($E_{1/2}$) of **AQ-1,8-3E-OH** is –0.43 V *vs.* SHE at pH 7 and –0.52 V at pH 14 (Figure S6). The Pourbaix diagram in Figure 3b shows the pH-dependence of its reduction potential; it is consistent with a transfer of 2 H^+/2 e^- from pH 5 to 10.8, 1 H^+/2 e^- from pH 10.8 to 12.6 and 0 H^+/2 e^- from pH 12.6 to 14. Similar pH-dependent behavior of the reduction potential has been observed for other anthraquinone derivatives in aqueous media[18, 34] (Figure S9). Therefore, when starting at pH 7, the reduced **AQ-1,8-3E-OH** will exist in three different forms, as shown in Figure 3a. As its electrochemical reaction is pH-dependent and reversible, upon charging (reducing) the negolyte, a process that takes protons up from water, the pH of the initially neutral solution is expected to increase until it reaches approximately pK_{a2}. After discharging, a process that releases protons into the negolyte, the neutral pH is expected to be fully recovered.

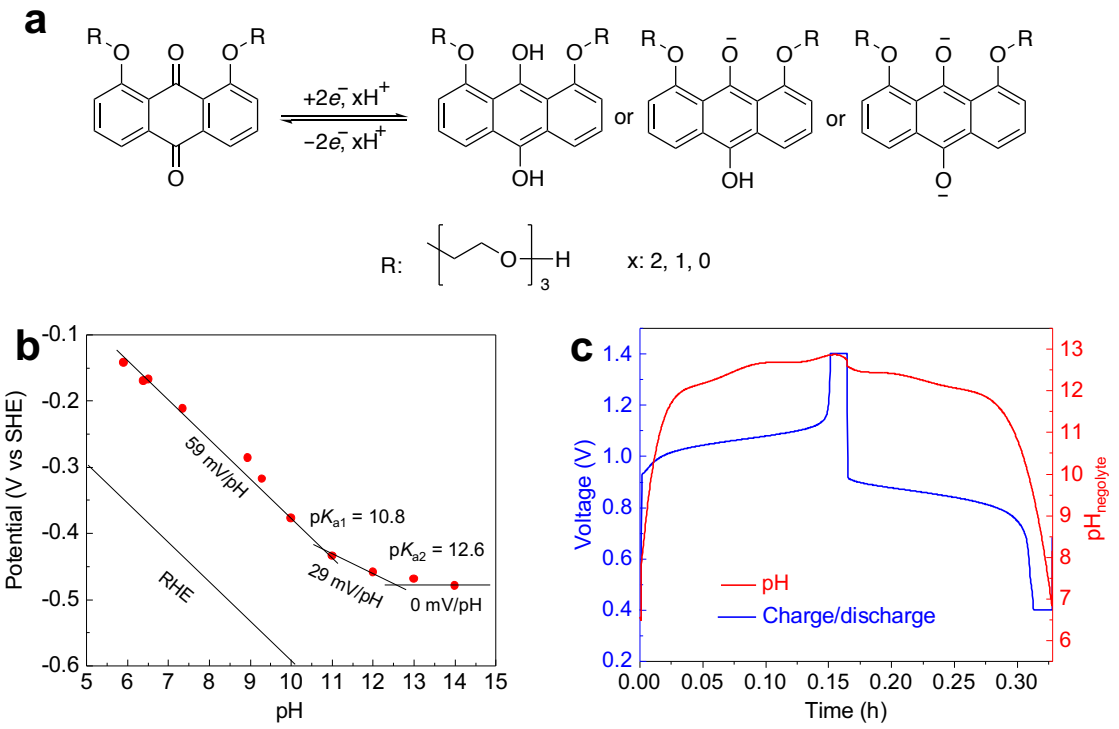

Figure 3 | pH related properties of AQ-1,8-3E-OH. (a) Scheme of the three different reduction products of the anthraquinone. (b) Pourbaix diagram of AQ-1,8-3E-OH with a line of constrained slope of –59 mV/pH fit to the data from pH 6-10 and a constrained slope of –29 mV/pH from pH 10-12.5. Above pH ~ 12.6, the potential is pH-independent, indicating that the reduced form of AQ-1,8-3E-OH is deprotonated. The lines of slope 59, 29, and 0 mV/pH are simply guides to the eye. All of the potentials were determined by cyclic voltammograms of 10 mM AQ-1,8-3E-OH in buffered solutions. (c) Charging of AQ-1,8-3E-OH increases the pH of the solution, and discharging reverses the pH change. Electrolytes comprised 7 mL of 0.1 M AQ-1,8-3E-OH (negolyte) in 1 M KCl and 40 mL of 0.1 M potassium ferrocyanide and 0.04 M potassium ferricyanide (posolyte) in 1 M KCl. The applied current density was 50 mA/cm^2.

Given the redox-activity and water-miscibility of **AQ-1,8-3E-OH** at pH 7, we investigated the performance of a PEGAQ-based flow cell with neutral electrolytes. To better understand the pH evolution during charge/discharge, we built a cell with 0.1 M electrolytes and tracked the pH of the negolyte during charge/discharge by immersing a pH probe in the negolyte (Figure 3c). To exclude the influence of oxygen dissolved in electrolytes on pH increase during charge, the electrolytes were first deaerated and then transferred to a glovebox filled with N_2[14]. In a full

cycle with close to 100% Coulombic efficiency, the pH increased from 7 to 12.8 during charging and returned from pH 12.8 to 7 during discharging, confirming the pH reversibility. Compared to strongly acidic or basic electrolytes, such less-corrosive electrolytes (pH = 7–13) are preferable in terms of less expensive electrolyte-contacting materials and structural stability of redox-active species[6, 11, 14, 35]. Based on the Pourbaix diagram in Figure 3b, the absence of a visible signature of pH swing in the charge/discharge curves in Figure 3c seems surprising. This may occur because the local pH at the electrode surface can shift immediately upon the commencement of charging and discharging, while the bulk pH changes over the longer time scale of the reservoir SOC tracked in Fig. 3c.

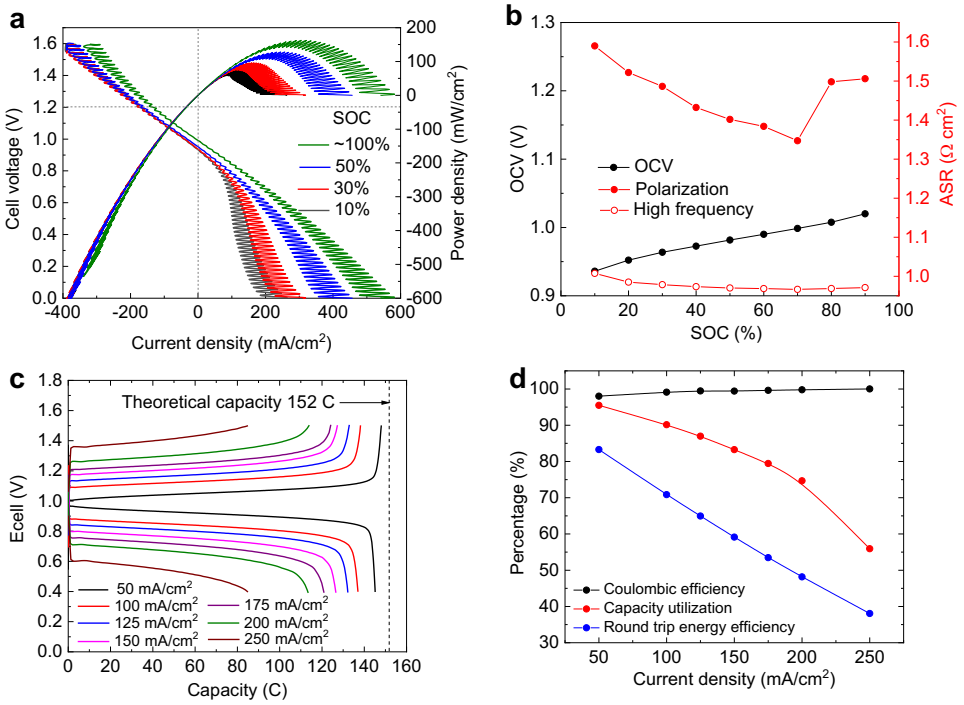

Figure 4 | Low-concentration flow battery performance. (a) Cell voltage and power density *vs.* current density at room temperature at 10%, 30%, 50%, and ~100% SOC. Electrolytes comprised 7.4 mL of 0.1 M AQ-1,8-3E-OH (negolyte) in 1 M KCl and 40 mL of 0.1 M potassium ferrocyanide and 0.04 M potassium ferricyanide (posolyte) in 1 M KCl. Current oscillations arise from peristaltic pumping. (b) OCV, high frequency and polarization AC-ASR *vs.* SOC. (c) Galvanostatic charge and discharge curves from 50 to 250 mA/cm² with 1.5 and 0.4 V cutoffs. The theoretical capacity is indicated by the vertical dashed line. (d) Coulombic efficiency, round-trip energy efficiency and capacity utilization as a percentage of theoretical capacity versus current density.

Polarization experiments were conducted at different SOC of the negolyte, and a peak power density of 0.18 W cm^{-2} was achieved at ~100% SOC (Figure 4a). The open-circuit voltage (OCV) increases from 0.94 V to 1.01 V as the SOC increases from 10% to 90%, and the OCV at 50% SOC was 0.98 V (Figure 4b). The alternating current area-specific resistance (AC-ASR) of the cell was determined via high-frequency electrochemical impedance spectroscopy (EIS) and the value was slightly lower than 1 Ω cm^2 across all SOCs (Figure 4b). The polarization ASR was determined using the linear region within the voltage range 0.9 to 1.1 V and the current range –50 to 50 mA (Figure 4a, b). The membrane resistance contributes more than 70% of the AC-

ASR of the entire cell. The capacity utilization decreased from 95% at 50 mA/cm^2 to 84 and 56% at 150 and 250 mA/cm^2, respectively (Figure 4c, d).

To exploit the water-miscibility of **AQ-1,8-3E-OH**, we constructed a full cell with a concentrated negolyte comprising 7 mL of 1.5 M **AQ-1,8-3E-OH** in 1 M KCl as the capacity-limiting side and posolyte comprising 150 mL of 0.31 M $K_4Fe(CN)_6$ with 0.31 M $K_3Fe(CN)_6$ in 1 M KCl as the non-capacity-limiting side. In Figure 5, we demonstrate a negolyte with the record volumetric capacity of 80.4 Ah/L. Furthermore, **AQ-1,8-3E-OH** becomes a liquid when the temperature exceeds 35 °C, in which case the theoretical limit of the volumetric capacity is 120.1 Ah/L, corresponding to pure **AQ-1,8-3E-OH** (molarity: 2.24 M); in practice, however, the capacity of a real cell would be limited by the addition of water and salt for conductivity. Polarization experiments were further conducted, and the cell showed a higher OCV across all SOCs than with the previous 0.1 M-negolyte cell (1.06 V at 50% SOC, Figure 5a and 5b); this difference is explained in the Supporting Information (p. 16). The high-frequency ASR in the high concentration cell (Figure 5b) is approximately 1.3 times that of the low concentration cell; we attribute this to the increased negolyte viscosity. **AQ-1,8-3E-OH** at 1.5 M possesses a viscosity of ~90 mPa·s at 37 °C, whereas the viscosity of a 0.1 M solution is only ~1 mPa·s (Figure S4-S5). The higher viscosity slows the mass transfer rate. Interestingly, an increase in viscosity of nearly two orders of magnitude does not incur proportional increases in either resistance or peak power density because of the countervailing influence of a twenty-fold increase in negolyte reactant concentration. The peak power density of 0.17 W/cm^2 achieved at ~100% SOC in the high concentration cell (Figure 5a) is only slightly lower than that in the low concentration cell. In contrast, lower capacity utilization was observed when the high-concentration cell was charged and discharged at varying current densities. The accessible capacity at 50 mA/cm^2 was only 84.7% in the high concentration cell (Figure S10), as a result of high-viscosity induced mass-transport limitations[36, 37], as opposed to 96% in the low concentration (0.1 M) cell. A higher viscosity would lead to increased pumping power losses for a given flow channel configuration and electrode porosity and thickness, but these parameters would be chosen differently for low and high viscosity electrolytes[38, 39].

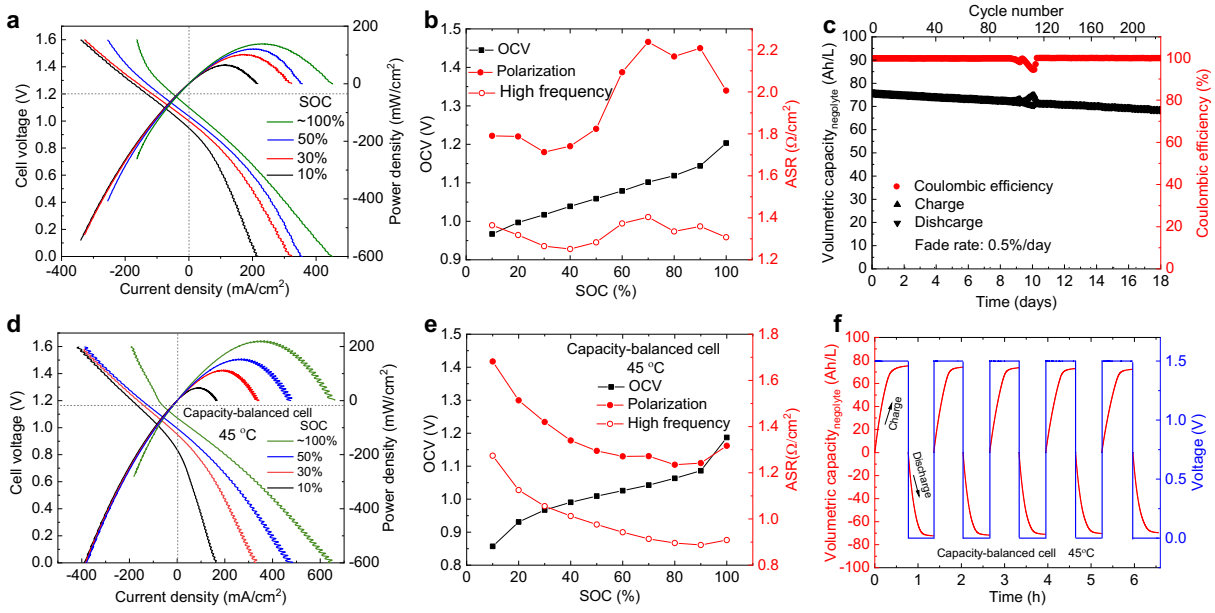

Figure 5 | High-concentration flow cell performance. (a) Cell voltage and power density *vs.* current density at room temperature at 10%, 30%, 50%, and ~100% SOC. Electrolytes comprised 7 mL of 1.5 M AQ-1,8-3E-OH (negolyte) in 1 M KCl and 150 mL of 0.31 M potassium ferrocyanide and 0.31 M potassium ferricyanide (posolyte) in 1 M KCl. (b) OCV, high frequency, and polarization ASR *vs.* SOC. (c) Current efficiency and charge/discharge capacities *vs.* time and cycle number. (d) Cell voltage and power density *vs.* current density at 45 °C at 10%, 30%, 50%, and ~100% SOC. Electrolytes comprised 6 mL of 1.5 M AQ-1,8-3E-OH (negolyte) in 0.5 M KCl and 12 mL of 1.51 M 1:1 mixed potassium/sodium ferrocyanide and 0.01 M potassium ferricyanide (posolyte) in DI water. (e) OCV, high frequency, and polarization ASR *vs.* SOC. (f) Charge/discharge under potentiostatic conditions.

Continuing to use the aforementioned cell setup and electrolytes, we performed a cycling experiment to evaluate the capacity fade rate by utilizing a sequential potential step method (Supplementary Information, Full Cell Measurements, p. 14). With this method, we accessed 95.7% of the theoretical capacity — the unutilized capacity might have been caused by a droplet electrolyte sticking on the wall of the electrolyte Falcon™ tube container or by a small amount of impurity in the sample. The achieved capacity utilization is comparable with that of prior work[12, 15]. The cell was run for 220 cycles over 18 days with an average current efficiency of 99.90% (Figure 5c). The current efficiency decreased to 97% from the 105th to the 120th cycle due to depletion of nitrogen gas in the glove bag but then increased to >99.95% when the nitrogen supply was refilled. Apparently, such a disturbance does not influence the capacity fade rate, as the reaction with atmospheric oxygen is apparently self-discharge and not decomposition. We then fitted the capacity fade rate by using a first-order exponential decay model to obtain a temporal fade rate constant of 0.5%/day or 0.043%/cycle. As the capacity of the posolyte is 2.2 times that of the negolyte, and the negolyte crossover rate is negligible according to our permeability measurements[11], we attribute the capacity fade exclusively to the decomposition of the active material in the negolyte. The decomposition product was identified, and possible decomposition pathways are proposed in the Supporting Information (Decomposition Analysis, pp. 17-27, Figure S11-S18).

We investigated increasing the energy density by pairing the 1.5 M negolyte with a more concentrated posolyte. Mixing potassium and sodium ferrocyanides in a 1:1 molar ratio[40], we were able to construct a capacity-balanced flow cell with 12 mL 1.51 M 1:1 mixed potassium/sodium ferrocyanide and 0.01 M potassium ferricyanide as the posolyte, and 6 mL 1.5 M **AQ-1,8-3E-OH** in 0.5 M KCl solution as the negolyte. The electrolyte reservoirs were immersed in a water bath and heated to 45 °C to prevent ferrocyanide precipitation. Polarization shows that the OCV at 50% SOC for this cell is 1.01 V (Figure 5e). Under elevated temperature, both high-frequency and polarization resistance are reduced significantly due to increased ion conductivity and reduced electrolyte viscosity. The peak power density of 0.22 W/cm^2, achieved at ~100% SOC, represents an approximately 30% increase compared to room temperature performance. Using potentiostatic methods, charging at 1.5 V and discharging at 0 V, the cell accessed 94% of the theoretical capacity, which implies an energy density of 25.2 Wh/L — one of the highest among all organic aqueous and non-aqueous flow batteries. Theoretically, if 2.2 M **AQ-1,8-3E-OH** were paired with capacity-balanced 1.5 M ferrocyanide[13, 40], an energy density of 30.0 Wh/L would be expected.

In summary, we introduce **AQ-1,8-3E-OH** as the first water-miscible negolyte molecule for ARFBs. We demonstrate the highest volumetric capacity (80.4 Ah/L) ever reported among all aqueous organic electrolytes. The theoretical capacity limit is 120.1 Ah/L for the neat 2.2 M liquid quinone. An energy density of 25.2 Wh/L was demonstrated when 1.5 M **AQ-1,8-3E-OH** was paired with 1.5 M ferrocyanide. The theoretical energy density is 30.0 Wh/L for a full cell with a 2.2 M negolyte and a capacity-balanced 1.5 M ferrocyanide posolyte. As a first step

toward developing lifetime extension strategies, post-mortem chemical analysis enabled us to identify the structure of a decomposition product and to propose four plausible degradation pathways. Further systematic exploration of PEG functionalizations may shed light on the development of low-cost, high-capacity, and high-stability RAMs for ARFBs.

Supporting Information

Table of recent aqueous and nonaqueous flow battery works, synthesis, characterization, and screening of PEGAQs, solubility measurements, electrochemical analysis, decomposition products analysis, and materials and methods.

Acknowledgments

This research was supported by U.S. DOE award DE-AC05-76RL01830 through PNNL subcontract 428977, by ARPA-E award DE-AR0000767, and by the Massachusetts Clean Energy Technology Center. We thank Prof. Luke Davis, Emily Kerr, Min Wu, Andrew Wong, Eric Fell, Winston Michalak, and James Niffenegger for useful discussions. D.A.P. acknowledges funding support from the NSF Graduate Research Fellowship Program, no. DGE1144152 and DGE1745303.

References

1. Moya, A. A. Electric Circuits Modelling the Low-frequency Impedance of Ideal Ion-exchange Membrane Systems. *Electrochimica Acta* **2012,** *62*, 296–304.
2. Rugolo, J.; Aziz, M. J. Electricity Storage for Intermittent Renewable Sources. *Energy & Environmental Science* **2012,** *5*, 7151.
3. Dunn, B.; Kamath, H.; Tarascon, J.-M. Electrical Energy Storage for the Grid: A Battery of Choices. *Science* **2011,** *334*, 9.
4. Plesset, M. S.; Helfferich, F.; Franklin, J. N. Ion Exchange Kinetics. A Nonlinear Diffusion Problem. II. Particle Diffusion Controlled Exchange of Univalent and Bivalent Ions. *The Journal of Chemical Physics* **1958,** *29* (5), 1064–1069.
5. Liu, W.; Lu, W.; Zhang, H.; Li, X. Aqueous Flow Batteries: Research and Development. *Chem. Eur. J.* **2018,** *24*, 17.
6. Soloveichik, G. L. Flow Batteries: Current Status and Trends. *Chem. Rev.* **2015,** *115* (20), 11533–58.
7. Li, L.; Kim, S.; Wang, W.; Vijayakumar, M.; Nie, Z.; Chen, B.; Zhang, J.; Xia, G.; Hu, J.; Graff, G.; Liu, J.; Yang, Z. A Stable Vanadium Redox-Flow Battery with High Energy Density for Large-Scale Energy Storage. *Adv. Energy Mater.* **2011,** *1*, 7.
8. Bauer, F.; Denneler, S.; Willert-Porada, M. Influence of Temperature and Humidity on the Mechanical Properties of Nafion® 117 Polymer Electrolyte Membrane. *Journal of Polymer Science Part B: Polymer Physics* **2005,** *43* (7), 786–795.
9. Yang, Z.; Tong, L.; Tabor, D. P.; Beh, E. S.; Goulet, M.-A.; Porcellinis, D. D.; Aspuru-Guzik, A.; Gordon, R. G.; Aziz, M. J. Alkaline Benzoquinone Aqueous Flow Battery for Large-Scale Storage of Electrical Energy. *Adv. Energy Mater.* **2018**, *8*, 1702056.
10. Dieterich, V. M.; Jarrod D.; Barton, John L.; Carney Thomas J.; Darling, Robert M.; Brushett, Fikile R. Estimating the Cost of Organic Battery Active Materials: A Case Study on Anthraquinone Disulfonic Acid. *Translational Materials Research* **2018**, *5*, 034001.
11. Kwabi, D. G.; Lin, K.; Ji, Y.; Kerr, E. F.; Goulet, M.-A.; Porcellinis, D. D.; Tabor, D. P.; Pollack, D. A.; Aspuru-Guzik, A.; Gordon, R. G.; Aziz, M. J. Alkaline Quinone Flow Battery with Long Lifetime at pH 12. *Joule* **2018,** *2* (9), 13.

12. Beh, E. S.; De Porcellinis, D.; Gracia, R. L.; Xia, K. T.; Gordon, R. G.; Aziz, M. J. A Neutral pH Aqueous Organic–Organometallic Redox Flow Battery with Extremely High Capacity Retention. *ACS Energy Lett.* **2017,** *2* (3), 639–644.
13. Luo, J.; Hu, B.; Debruler, C.; Bi, Y.; Zhao, Y.; Bing, Y.; Hu, M.; Wu, W.; Liu, T. L. Unprecedented Capacity and Stability of Ammonium Ferrocyanide Catholyte in pH Neutral Aqueous Redox Flow Batteries. *Joule* **2019,** *3*, 149–163.
14. Ji, Y.; Goulet, M-A.; Pollack, D. A.; Kwabi, D. G.; Jin, S.; De Porcellinis, D.; Kerr, E. F.; Gordon, R. G.; Aziz, M. J. A Phosphonate-Functionalized Quinone Redox Flow Battery at Near-Neutral pH with Record Capacity Retention Rate. *Adv. Energy Mater.* **2019**, *9*, 1900039.
15. Hollas, A.; Wei, X.; Murugesan, V.; Nie, Z.; Li, B.; Reed, D.; Liu, J.; Sprenkle, V.; Wang, W. A Biomimetic High-Capacity Phenazine-Based Anolyte for Aqueous Organic Redox Flow Batteries. *Nature Energy* **2018,** *3* (6), 508–514.
16. Dominijanni, A.; Manassero, M. Modelling the Swelling and Osmotic Properties of Clay Soils. Part II: The Physical Approach. *International Journal of Engineering Science* **2012,** *51*, 51–73.
17. DeBruler, C.; Hu, B.; Moss, J.; Luo, J.; Liu, T. L. A Sulfonate-Functionalized Viologen Enabling Neutral Cation Exchange, Aqueous Organic Redox Flow Batteries Toward Renewable Energy Storage. *ACS Energy Lett.* **2018,** *3* (3), 663–668.
18. Huskinson, B.; Marshak, M. P.; Suh, C.; Er, S.; Gerhardt, M. R.; Galvin, C. J.; Chen, X.; Aspuru-Guzik, A.; Gordon, R. G.; Aziz, M. J. A Metal-free Organic-Inorganic Aqueous Flow Battery. *Nature* **2014,** *505* (7482), 195–8.
19. Kusoglu, A.; Santare, M. H.; Karlsson, A. M. Mechanics-based Model for Non-affine Swelling in Perfluorosulfonic Acid (PFSA) Membranes. *Polymer* **2009,** *50* (11), 2481–2491.
20. Janoschka, T.; Martin, N.; Hager, M. D.; Schubert, U. S. An Aqueous Redox-Flow Battery with High Capacity and Power: The TEMPTMA/MV System. *Angew. Chem. Int. Ed.* **2016,** *55* (46), 14427–14430.
21. Wang, C.; Yang, Z.; Wang, Y.; Zhao, P.; Yan W.; Zhu, G.; Ma, L.; Wang, L.; Li, G.; Liu, J.; Jin, Z. High-performance Alkaline Organic Redox Flow Batteries Based on 2-hydroxy-3-carboxy-1,4-naphthoquinone. *ACS Energy Lett.* **2018,** *3*, 6.
22. Lin, K.; Chen, Q.; Gerhardt, M. R.; Tong, L.; Kim, S. B.; Eisenach, L.; Valle, A. W.; Hardee, D.; Gordon, R. G.; Aziz, M. J.; Marshak, M. P. Alkaline Quinone Flow Battery. *Science* **2015,** *349* (6255), 5.
23. Lin, K.; Gómez-Bombarelli, R.; Beh, E. S.; Tong, L.; Chen, Q.; Valle, A.; Aspuru-Guzik, A.; Aziz, M. J.; Gordon, R. G. A Redox-flow Battery with an Alloxazine-based Organic Electrolyte. *Nature Energy* **2016,** *1* (9), 16102.
24. Suttil, J. A.; Kucharyson, J. F.; Escalante-Garcia, I. L.; Cabrera, P. J.; James, B. R.; Savinell, R. F.; Sanford, M. S.; Thompson, L. T. Metal Acetylacetonate Complexes for High Energy Density Non-aqueous Redox Flow Batteries. *Journal of Materials Chemistry A* **2015,** *3* (15), 7929–7938.
25. Kwon, G.; Lee, S.; Hwang, J.; Shim, H.-S.; Lee, B.; Lee, M. H.; Ko, Y.; Jung, S.-K.; Ku, K.; Hong, J.; Kang, K. Multi-redox Molecule for High-Energy Redox Flow Batteries. *Joule* **2018**, 2, 1771–1782.
26. Hu, B.; Liu, T. L. Two Electron Utilization of Methyl Viologen Anolyte in Nonaqueous Organic Redox Flow Battery. *Journal of Energy Chemistry* **2018,** *27* (5), 1326–1332.
27. Yang, B.; Hoober-Burkhardt, L.; Wang, F.; Surya Prakash, G. K.; Narayanan, S. R. An Inexpensive Aqueous Flow Battery for Large-scale Electrical Energy Storage Based on Water-

soluble Organic Redox Couples. *Journal of the Electrochemical Society* **2014,** *161*, A1371–A1380.
28. Wei, X.; Duan, W.; Huang, J.; Zhang, L.; Li, B.; Reed, D.; Xu, W.; Sprenkle, V.; Wang, W. A High-current, Stable Nonaqueous Organic Redox Flow Battery. *ACS Energy Letters* **2016,** *1* (4), 705–711.
29. Hu, B.; DeBruler, C.; Rhodes, Z.; Liu, T. Leo Long-cycling Aqueous Organic Redox Flow Battery (AORFB) Toward Sustainable and Safe Energy Storage. *Journal of the American Chemical Society* **2017,** *139* (3), 1207–1214.
30. Wei, X.; Xu, W.; Huang, J.; Zhang, L.; Walter, E.; Lawrence, C.; Vijayakumar, M.; Henderson, W. A.; Liu, T.; Cosimbescu, L.; Li, B.; Sprenkle, V.; Wang, W. Radical Compatibility with Nonaqueous Electrolytes and Its Impact on an All-organic Redox Flow Battery. *Angew. Chem. Int. Ed.* **2015,** *54* (30), 8684–7.
31. Huskinson, B.; Marshak, M. P.; Gerhardt, M. R.; Aziz, M. J. Cycling of a Quinone-Bromide Flow Battery for Large-Scale Electrochemical Energy Storage. *ECS Transactions* **2014,** *61* (37), 27–30.
32. Ponce de León, C.; Frías-Ferrer, A.; González-García, J.; Szánto, D. A.; Walsh, F. C. Redox Flow Cells for Energy Conversion. *Journal of Power Sources* **2006,** *160* (1), 716–732.
33. Giguere, J. B.; Morin, J. F. New Strapped Porphyrins as Hosts for Fullerenes: Synthesis and Complexation Study. *Org. Biomol. Chem.* **2012,** *10* (5), 1047–51.
34. Quan, M.; Sanchez, D.; Wasylkiw, M. F.; Smith, D. K. Voltammetry of Quinones in Unbuffered Aqueous Solution: Reassessing the Roles of Proton Transfer and Hydrogen Bonding in the Aqueous Electrochemistry of Quinones. *Journal of American Chemical Society* **2007,** *129*, 12847–12856.
35. Silberstein, M. N.; Boyce, M. C. Constitutive Modeling of the Rate, Temperature, and Hydration Dependent Deformation Response of Nafion to Monotonic and Cyclic Loading. *Journal of Power Sources* **2010,** *195* (17), 5692–5706.
36. Chen, Q.; Gerhardt, M. R.; Aziz, M. J. Dissection of the Voltage Losses of an Acidic Quinone Redox Flow Battery. *Journal of The Electrochemical Society* **2017,** *164* (6), A1126–A1132.
37. Milshtein, J. D.; Tenny, K. M.; Barton, J. L.; Drake, J.; Darling, R. M.; Brushett, F. R. Quantifying Mass Transfer Rates in Redox Flow Batteries. *J. Electrochem. Soc.* **2017,** *164*, E3265–E3275.
38. Milshtein, J. D.; Darling, R. M.; Drake, J.; Perry, M. L.; Brushett, F. R. The Critical Role of Supporting Electrolyte Selection on Flow Battery Cost. *Journal of The Electrochemical Society* **2017,** *164* (14), A3883–A3895.
39. Gerhardt, M. R.; Wong, A. A.; Aziz, M. J. The Effect of Interdigitated Channel and Land Dimensions on Flow Cell Performance. *Journal of The Electrochemical Society* **2018,** *165* (11), A2625–A2643.
40. Nemat-Nasser, S. Micromechanics of Actuation of Ionic Polymer-Metal Composites. *Journal of Applied Physics* **2002,** *92* (5), 2899–2915.